Direct Nano-Synthesis Methods Notably Benefit Mg-Battery Cathode Performance

Lauren E. Blanc, Xiaoqi Sun, Abhinandan Shyamsunder, Victor Duffort, Linda F. Nazar

Direct Nano-synthesis Methods Notably Benefit Mg-Battery Cathode Performance

*Lauren E. Blanc,[a†] Xiaoqi Sun,[§,a†] Abhinandan Shyamsunder,[a] Victor Duffort,[a,‡] and Linda F. Nazar[a]**

[a]*Joint Center for Energy Storage Research, Department of Chemistry and the Waterloo Institute for Nanotechnology, University of Waterloo, Waterloo Ontario Canada N2L 3G1*

[§]Current address: Department of Chemistry, Northeastern University, Shenyang, China, 110819

[‡]Current address: Univ. Lille, CNRS, Centrale Lille, ENSCL, Univ. Artois, UMR 8181, UCCS-Unitée de Catalyse et Chimie du Solide, F-59000, Lille, France

[†] These authors contributed equally

*E-mail: lfnazar@uwaterloo.ca

Keywords: Magnesium battery, nano-dimensional, sulfide cathode, energy storage, intercalation, conversion

Abstract:

Rechargeable magnesium batteries are promising candidates for next-generation electrochemical energy storage, but their development is severely hindered by sluggish solid-state diffusion and significant desolvation penalties of the divalent cation. Studies suggest that nano-sized electrode materials alleviate these issues by shortening diffusion lengths and increasing electrode/electrolyte interaction. Here, we investigate the effect of particle size and synthetic methodology on the electrochemical performance of four sulfide cathode materials in Mg batteries: layered TiS_2, CuS, spinel Ti_2S_4 and $CuCo_2S_4$. In these sulfide hosts, the direct preparation of nano-dimensional crystallites is critical to activate or improve electrochemistry. Even promising cathode materials can appear electrochemically inert when micron-sized particles are investigated (e.g. $CuCo_2S_4$), and mechanical milling leads to surface degradation of active material which severely limits performance. However, nano-sized $CuCo_2S_4$ prepared directly reaches a capacity nearly double that of ball milled material and delivers 350 mAh g^{-1} at 60 °C. This work provides synthetic considerations which may be crucial in the discovery and design of novel Mg cathode materials so that promising candidates are not overlooked. By extension, in oxide materials where Mg^{2+} diffusion is expected to be much more sluggish, this factor is anticipated to be even more important when screening for new hosts.

Introduction:

Overconsumption of fossil fuels has led to a plethora of environmental issues and an impending energy crisis. To reduce carbon-based emissions, energy storage technology needs to be developed to (1) facilitate a transition from gasoline powered cars to electric vehicles and (2) integrate renewable power sources into the grid.[1–3] Rechargeable batteries offer viable approaches to achieve these goals, but improvements are needed to progress beyond current state of the art lithium ion batteries (LIBs) which are limited by economic factors and safety concerns.[4–6] As an earth-abundant metal and divalent cation, magnesium-based battery technology provides large theoretical volumetric energy densities at a fraction of the cost of LIBs.[7,8] Furthermore, rechargeable magnesium batteries are promising candidates for electrochemical energy storage due to limited dendritic growth and good safety of the Mg metal anode.[9–12]

Despite these desirable qualities, there are major challenges hindering the development of Mg batteries due to kinetic limitations associated with the transport and electrodeposition of the divalent cation.[13,14] While much progress has been made to increase the anodic stability and improve the efficiency of advanced Mg electrolytes,[15–17] the paucity of known cathode materials capable of reversible Mg^{2+} (de)insertion continues to plague this technology. High voltage oxides generally suffer from sluggish Mg^{2+} diffusion due to strong ionic interactions between the migrating cation and the highly polarizing lattice.[18–20] In these oxide materials, the desolvation process at the cathode/electrolyte interphase has been shown to add an additional kinetic barrier to intercalation,[21–23] and a strong driving force towards conversion has been widely observed.[11,24–28] Although sulfide cathodes offer a lower energy density than oxides, they exhibit weaker interactions with the divalent cation and allow for more facile solid diffusion. As a result, most successful magnesium ion batteries have been prepared by balancing a sulfide cathode material with a Mg metal anode. Reversible Mg^{2+} intercalation was first demonstrated by Aurbach *et al.* with the Chevrel phase Mo_6S_8 as the host,[29] while we later proved that the spinel and layered phases of titanium sulfides were excellent Mg cathode candidates.[30,31] We also demonstrated that CuS cathode materials uptake Mg *via* a conversion reaction; however, high temperatures were required to cycle most of the capacity of micron-sized material.[32]

Although these sulfide hosts provide better kinetics for Mg^{2+} insertion/diffusion in comparison to oxides, their electrochemical performance requires further improvement to compete with existing technology. One potential solution is to reduce the particle size of the cathode material to allow shorter ion diffusion lengths and enhance ingress/egress of Mg^{2+} ions by increasing the surface area exposed to the electrolyte. This strategy has been implemented to activate Li^+ insertion into olivine $LiMnPO_4$[33,34] and to improve the electrochemistry of other Li-ion[35–42] as well as Mg electrode materials.[43–47] Nanomaterials can either be prepared (1) directly through rapid, low-temperature syntheses that limit the growth of crystallites or (2) the particle size of micron-materials can be reduced with mechanical milling processes. While a wide variety of synthetic methods have been developed to directly prepare nano-sized oxide and binary sulfide materials, most ternary sulfides are prepared with a high-temperature solid state synthesis that produces micron-sized particles.[48–50] In

these cases, nano-sized particles must be obtained post-synthesis through a mechanical ball milling process.

Herein, we investigate the effect of crystallite size on the performance of four model Mg cathode candidates (layered TiS_2, CuS, spinel Ti_2S_4 and $CuCo_2S_4$), and critically analyze the impact each method of nano-sizing has on the materials' electrochemistry. We show that the electrochemical performance of both intercalation (titanium sulfides) and conversion (CuS and $CuCo_2S_4$) cathodes is a very strong function of particle size, but that advantages of nano-sizing are accompanied by negative consequences when micron-sized particles are subjected to mechanical milling. Even though decreasing the particle size of electrode materials enhances the risk of parasitic side-reactions and reduces their overall volumetric density due to less efficient packing,[51–53] this is not a major concern for the current stage of Mg battery research. The discovery of new candidates and improvement of their electrochemistry are more urgent goals to provide a platform to understand the fundamentals of multivalent cation insertion and guide further directions for research. Our study demonstrates that (1) the discovery of novel higher voltage cathodes likely requires first curtailing their crystallite sizes to nano-dimensions in order to avoid overlooking potential materials, and (2) optimal performance is obtained through direct nano-synthetic techniques.

Results and Discussion:

A wide variety of liquid-based approaches can be used to directly synthesize nano-sized binary sulfides. Two common Mg cathode materials, TiS_2 and CuS,[31,32] were prepared using wet syntheses (WS) in order to examine both intercalation and conversion electrodes, respectively (**Figure 1**). Nano-dimensional layered TiS_2 was prepared through a liquid phase synthesis (WS) in oleylamine (at 300 °C), resulting in particle sizes around 100 nm as shown in **Figure 1b**.[54] CuS nano-rods (prepared by a low temperature wet synthesis) aggregated into ~300 nm spheres (**Figure 1d**).[55] XRD patterns of WS-TiS_2 and WS-CuS confirm that each target phase was successfully prepared, (**Figure 1a, c**), and the peak broadening observed is due to the small coherence length of the crystallites produced using the wet synthesis technique.

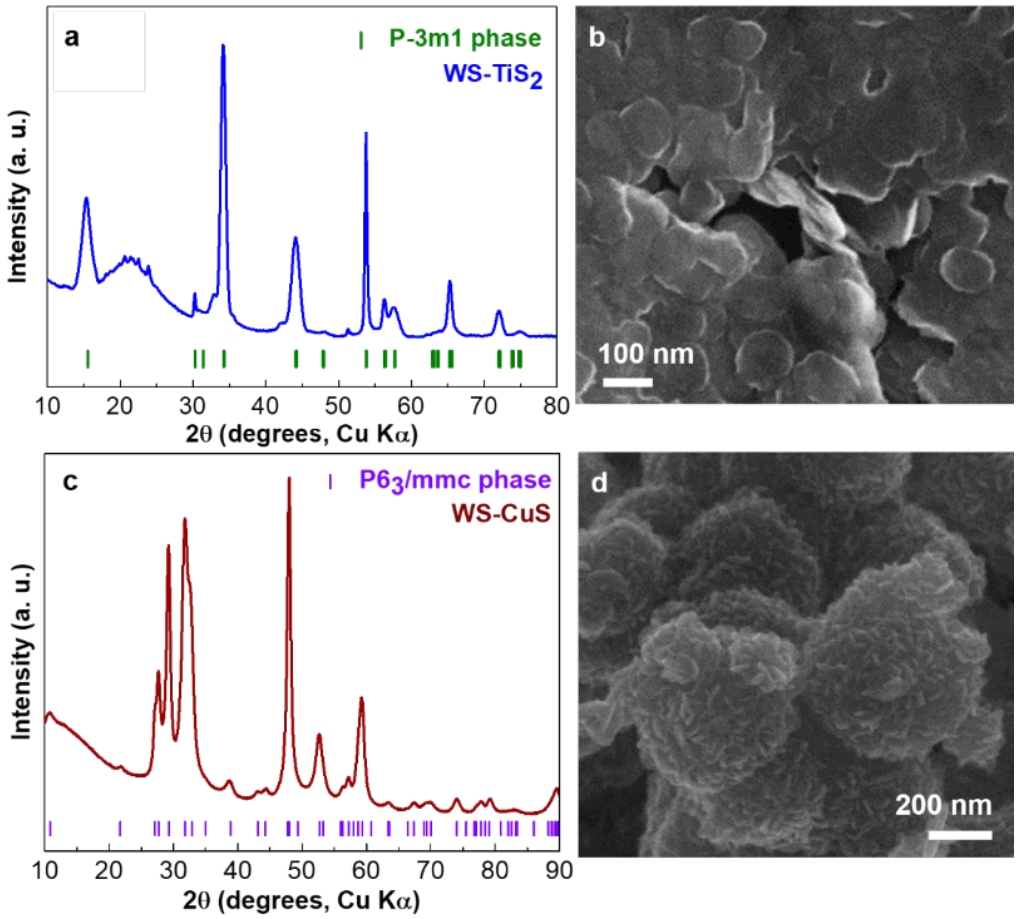

Figure 1: XRD patterns and SEM images of nano-sized (a, b) TiS_2 and (c, d) CuS prepared using wet synthesis.

As expected, nano-sized WS-TiS_2 and WS-CuS exhibit enhanced electrochemical performance in comparison to their micron counterparts (**Figure 2**). As reported in our previous work, micron-sized TiS_2 is an intercalation Mg cathode material which exhibits Mg^{2+} trapping after the first cycle, leading to 47% irreversible capacity at a current density of 12 mA g^{-1} (C/40 with 1C = 1 Mg^{2+}/TiS_2) and 60 °C.[31] This capacity loss is reduced by using nano-sized material, which exhibits only 15% irreversible capacity after the first cycle and further decreases to 8% after the second (**Figure 2a**). This electrochemical performance of WS-TiS_2 displays significant improvement - yielding larger initial discharge capacities (**Figure S1**) and better capacity retention - in comparison to the bulk material (**Figure 2a, b**). At a current density of 12 mA g^{-1}, micron-sized TiS_2 only reaches an initial discharge capacity of 270 mAh g^{-1} which fades considerably to 160 mAh g^{-1} upon further cycling (*vs*. 294 and 269 mAh g^{-1} for WS-TiS_2).[31]

The stepwise voltage profile of WS-TiS_2 shown in **Figure 2a** indicates a similar Mg^{2+} insertion process as the micron-sized material, although the difference in length of each plateau reflects some change in kinetics upon decreasing the particle size. Long term cycling of WS-TiS_2 at 60 °C at a current density of 48 mA g^{-1} shows that the material exhibits a fairly stable capacity and retains 120 mAh g^{-1} at the 200th cycle (**Figure 2b**). Under these conditions, the capacity of micron-sized TiS_2 fades to a comparable value after only 40 cycles.[31] Unlike micron-TiS_2 which exhibits extremely poor

electrochemistry at room temperature, the nano material also shows promising electrochemical properties at 25 °C. The larger initial capacity and better capacity retention of WS-TiS_2 compared to micron-TiS_2 is a direct result of shorter Mg^{2+} ion diffusion length.

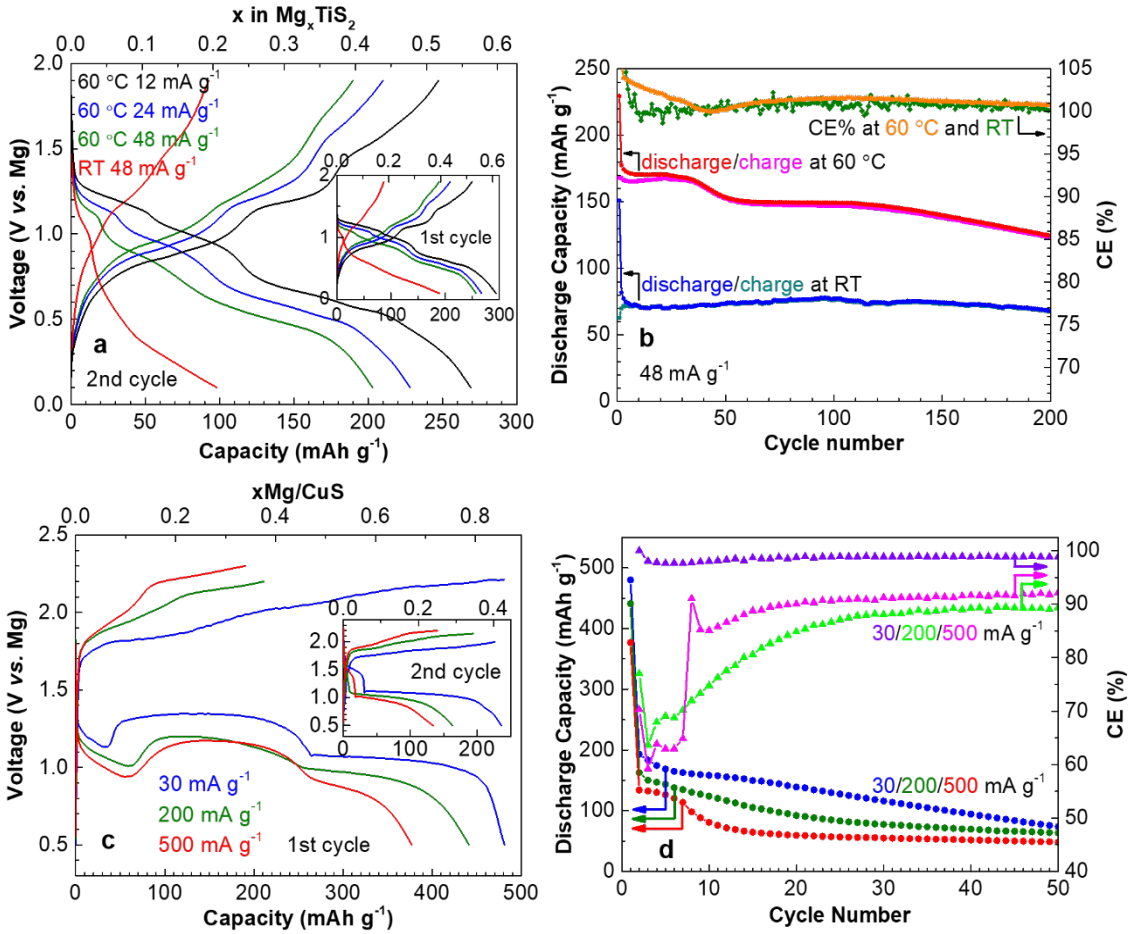

Figure 2: (a, b) Voltage profiles at various current densities and (c, d) capacity retention of WS-TiS_2 at 60 °C/RT and WS-CuS at 25 °C, respectively. Room temperature data were collected using APC/THF, while capacity retention data at 60 °C were obtained with APC/G4 electrolyte.

We have previously demonstrated that micron-sized CuS functions as a Mg cathode by conversion chemistry; however, an elevated temperature of 150 °C was required to approach reasonable capacities.[32] Decreasing the particle size through a low-temperature liquid synthesis approach creates more accessibility of the electrode surface by the electrolyte and promotes reactivity, enhancing electrochemical performance without the requirement of elevated temperatures. **Figure 2c** shows the voltage profiles of the nano-sized WS-CuS cathode in a Mg cell at room temperature. On discharge at a current density of 30 mA g^{-1} (C/19 with 1C = 1Mg^{2+}/CuS), two voltage plateaus at 1.4 V and 1.1 V are observed, each contributing to half of the 480 mAh g^{-1} overall capacity. The initial overpotential exhibited in the discharge profiles is likely the result of nucleation. *In situ* XRD demonstrates that two conversion reactions take place during the first and second plateaus of the first discharge (**Figure 3**):

$$CuS + 0.5Mg \rightarrow 0.5Cu_2S + 0.5MgS \quad (1)$$

$$0.5Cu_2S + 0.5Mg \leftrightarrow Cu + 0.5MgS \quad (2)$$

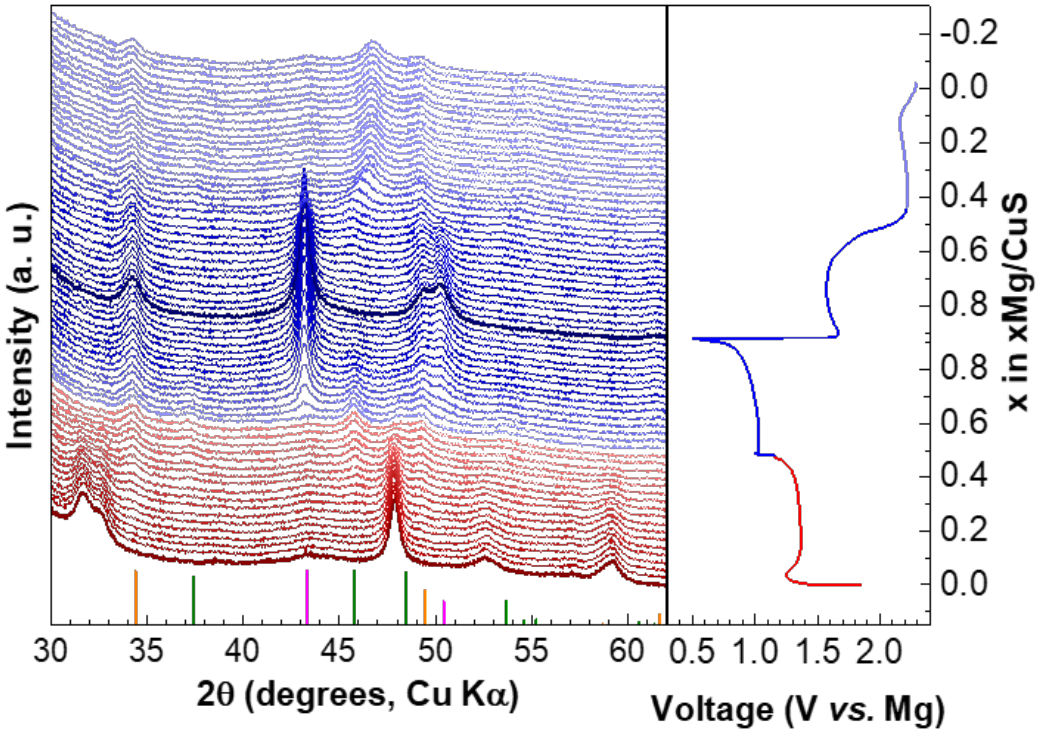

Figure 3: In situ XRD of CuS cycled in APC/THF with a Mg anode at room temperature and 30 mA g^{-1} current density. Red patterns correspond to the first voltage plateau and blue patterns correspond to the reversible second voltage plateau. The initial and fully discharge patterns are shown in dark red and dark blue, respectively. The appearance and disappearance of the MgS (orange), Cu_2S (green) and Cu (pink) phases demonstrates a conversion reaction.

This mechanism agrees with our previous report on micron-CuS at an elevated temperature.[32] After the first charge, the XRD pattern is similar to the one obtained at the end of the first discharge plateau (corresponding to Cu_2S and MgS) while the CuS starting phase is not observed (**Figure 3**). This suggests that only the lower voltage process (Equation 2) is reversible and that the irreversible nature of Equation 1 leads to the large capacity decay observed on the second cycle (**Figure 2c** inset).

Long term cycling of WS-CuS was carried out with a lower voltage cutoff corresponding to the end of the first charge plateau (**Figure 2d**). At a current density of 30 mA g^{-1}, the capacity drops from 193 mAh g^{-1} obtained on the second discharge, to 150 mAh g^{-1} maintained on the 50th cycle. Although initial capacities are lower, the capacity decay is slower with higher current densities of 200 mA g^{-1} and 500 mA g^{-1}, suggestive of suppressed parasitic reactions at the faster rates. *Ex situ* XPS on the Mg anode at the end of charge revealed a Cu signal (**Figure S2**), indicating that Cu dissolution and migration to the anode takes place during cycling which is a common challenge of conversion-type chalcogenide cathodes.[56] This loss of active material contributes to the capacity decay so that a faster cycling rate allows less time for such process and results in more stable capacity retention. Thus, the

electrochemical performance of nano-sized CuS can be optimized by preparing electrodes and/or designing cells in manners that minimize Cu shuttling in order to prevent this source of capacity fade. Furthermore, CuS particle morphologies with minimal agglomeration, in addition to small particle size, show exceptional promise as they exhibit reversible capacities with an impressive cycle life.[57,58] These results agree with other reports of nano-CuS prepared through a variety of methods: enhanced Mg^{2+} diffusion kinetics leads to improved electrochemical performance which can be obtained by using nanoparticles to prepare Mg electrodes.[59,60]

These results confirm that directly preparing nano-sized binary sulfides through a liquid synthetic route significantly improves electrochemical performance; however, this approach is not always applicable for the preparation of ternary sulfides. For example, $CuTi_2S_4$ is a ternary sulfide that can be oxidized to remove Cu ions and prepare spinel Ti_2S_4, a well-known host for Mg^{2+} intercalation.[30] This material is almost exclusively prepared *via* a conventional solid-state method, resulting in micron-sized particles. Here, these were subjected to mechanical ball milling (BM) to reduce particle size prior to electrochemical characterization. XRD confirms that BM-Ti_2S_4 retains its spinel structure, where the broadening of peaks is a result of the defects created during this high energy process (**Figure 4a**). **Figure 4b** shows a decrease in particle size from the original micron-sized particles (inset) to less than 1 µm which significantly shortens the Mg^{2+} diffusion length by a factor of ~10.

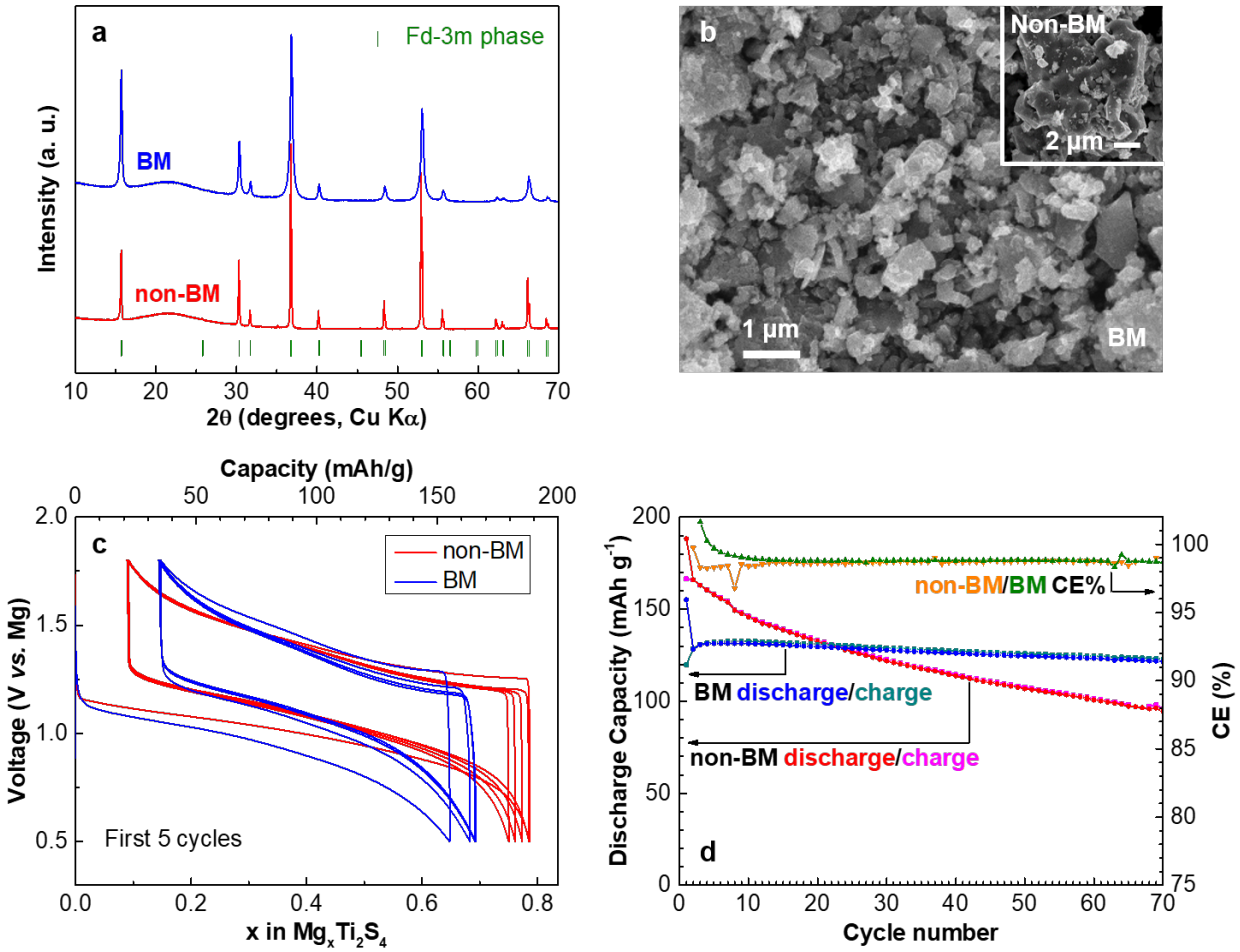

Figure 4: Comparison between micron-sized (non-BM) and ball milled (BM) spinel Ti_2S_4. (a) XRD, (b) SEM, (c) Voltage profiles of the first five cycles and (d) capacity retention of Ti_2S_4 cathodes with a Mg anode and APC/G4 electrolyte cycled at a current density of 48 mA g^{-1} and 60 °C.

While BM-Ti_2S_4 does show improved capacity retention in comparison to the micron-sized material, the nanomaterial actually exhibits a lower initial discharge capacity than bulk Ti_2S_4 (**Figure 4c, d**). This decreased discharge capacity is a result of surface degradation of the active material during the high energy milling process. Despite its limited capacity, after initial conditioning, BM-Ti_2S_4 shows a much lower capacity decay rate of only 0.13% per cycle, and it maintains 120 mAh g^{-1} capacity at the end of 70 cycles at a current density of 48 mA g^{-1} (C/5 with 1C = 1Mg^{2+}/Ti_2S_4) at 60 °C. This performance is significantly improved compared to the 0.7% capacity decay rate and 95 mAh g^{-1} capacity retained after the 70th cycle for the non-ball milled material under the same conditions. These results indicate that nano-sizing materials through mechanical milling has some positive impact on electrochemical performance; however, benefits are accompanied by significant negative consequences due to (1) surface degradation inhibiting Mg^{2+} ingress/egress into/from the structure and (2) the possibility of introducing impurities, thus lowering the capacity of active material (**Figure S3**).

The electrochemical performance of known cathodes indicates that both intercalation and conversion materials benefit significantly from a direct nano-synthesis. WS-TiS_2 and WS-CuS both exhibit increased capacities and better capacity retention as a result of the small particle size produced from their liquid synthesis. However, high energy processes to reduce particle size post-synthesis (e.g. ball milling) can have negative consequences on electrodes, as BM-Ti_2S_4 begins with a lower initial capacity *vs.* bulk material. To directly assess the degree to which synthetic methodology impacts electrochemical performance, nano-sized $CuCo_2S_4$ was obtained both by ball milling bulk material and through a direct nano-synthesis (**Figure 5**).

Spinel $CuCo_2S_4$ is isostructural with $CuTi_2S_4$; however extraction of Cu ions from the former is not possible, probably owing to the lowering of the S 3p level below that of the Co 3d band. [61] We thus examined $CuCo_2S_4$ itself as a cathode material. $CuCo_2S_4$ prepared from a conventional solid state synthesis contains a small amount of CoS_2 impurity and particle sizes are typically >10 µm (**Figure 5c, d**). As prepared, micron-sized $CuCo_2S_4$ requires an elevated temperature of 150 °C to exhibit any electrochemical activity. At this temperature and a current density of 10 mA g^{-1} (C/17 with 1C = 1Mg^{2+}/$CuCo_2S_4$), the bulk material has an initial discharge capacity of 60 mAh g^{-1}. Upon mechanical milling, the particle sizes decrease to hundreds of nanometers (**Figure 5d**) which allows the cathode to be cycled at lower temperatures. At the same current density, BM-$CuCo_2S_4$ has a promising capacity of 180 mAh g^{-1} at only 60 °C and even exhibits some activity at room temperature (**Figure 5e**). Reducing the particle size of $CuCo_2S_4$ has clear advantages in comparison to bulk material; however, these are not the best results that this material is capable of delivering. To achieve enhanced electrochemical performance, nano-sized $CuCo_2S_4$ was directly prepared using a low temperature melt approach reported by Khan, *et al*.[62] Stoichiometric mixtures of Cu(I) and Co(II) ethylxanthate salts were ground and decomposed at 250 °C to produce X-$CuCo_2S_4$. This approach generates a highly porous network of nano-sized $CuCo_2S_4$ particles (**Figure 5a, b**). When cycled at 10 mA g^{-1} and 60 °C, X-$CuCo_2S_4$ reaches an initial discharge capacity of 350 mAh g^{-1}, nearly double that of BM-$CuCo_2S_4$.

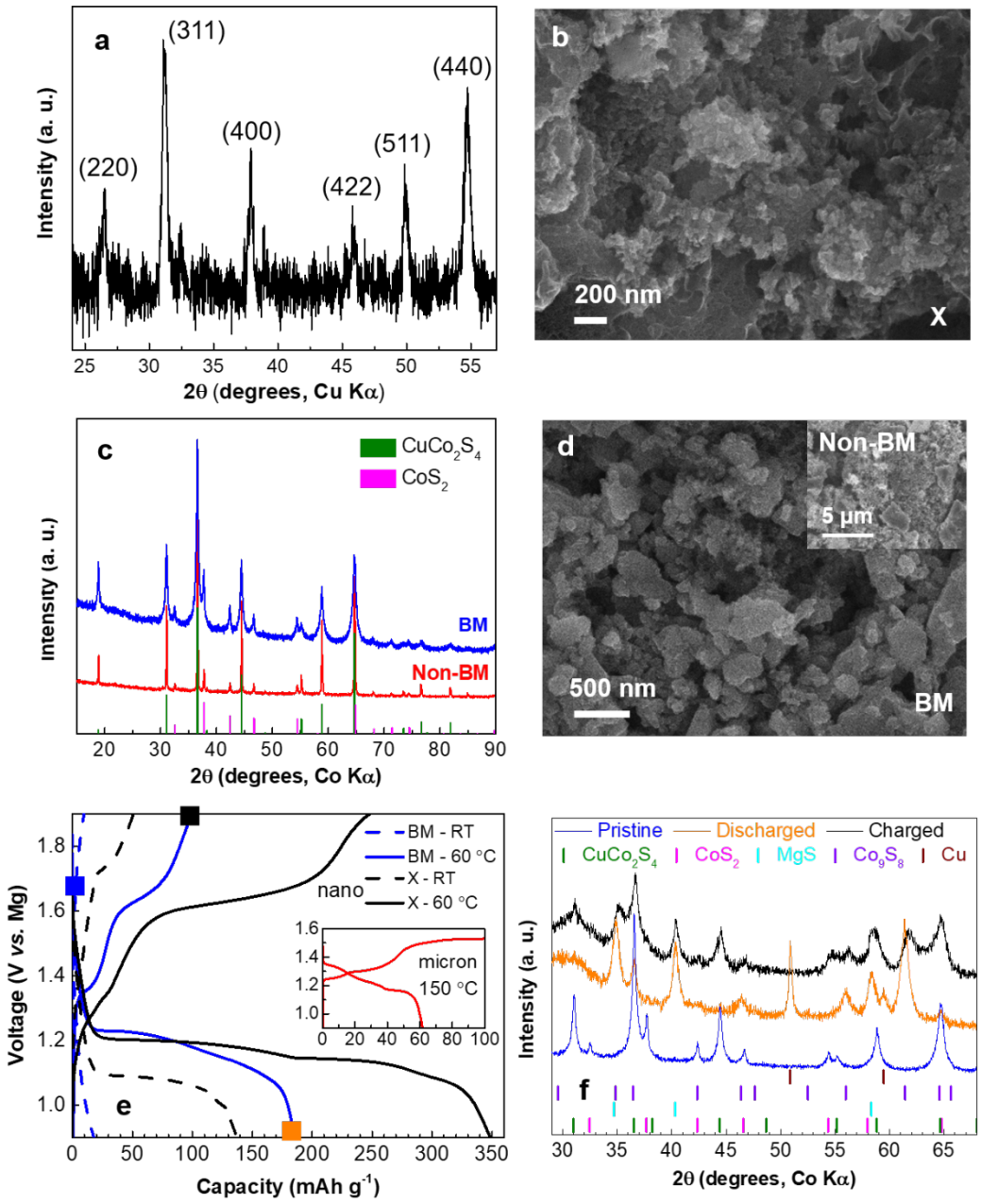

Figure 5: (a) XRD pattern and (b) SEM image of X-$CuCo_2S_4$ prepared using the xanthate method. (c) XRD patterns and (d) SEM images of micron-sized $CuCo_2S_4$ prepared through a solid state synthesis and then ball milled (BM) to reduce particle size. (e) Voltage profiles of X-, BM- and micron-$CuCo_2S_4$ cycled at 10 mA g^{-1} with a Mg anode at a variety of temperatures. Room temperature (RT) and 60 °C data were collected using APC/THF while 150 °C data was collected using APC/G4 electrolyte. Squares in black, blue and orange correspond to the points where XRD patterns were collected, shown in: f) Ex situ XRD of BM-$CuCo_2S_4$ cycled at 10 mA g^{-1} and 90 °C, demonstrating a conversion mechanism.

The capacities observed for nano-sized materials at elevated temperature are higher than $1Mg^{2+}/CuCo_2S_4$, which renders intercalation an unlikely mechanism, and thus *ex situ* XRD was carried out to study the structural change of the cathode upon cycling (**Figure 5f**). At the end of discharge,

spinel peaks disappear and MgS, Co_9S_8 and Cu phases are formed. This suggests a conversion reaction takes place:

$$CuCo_2S_4 + 2.22Mg^{2+} + 4.44e^- \rightarrow 2.22MgS + 0.22Co_9S_8 + Cu \quad (3)$$

which gives rise to the high capacity of 350 mAh g^{-1}, close to the theoretical value of 384 mAh g^{-1}. The Mg^{2+} intercalation barrier in $CuCo_2S_4$ might be due to Cu ions blocking the migration tunnel in the spinel structure so that the conversion reaction is more favorable. However, multiple discharge plateaus appear in the voltage profile, indicating that several individual electrochemical processes take place and the overall mechanism is more complicated than suggested by Equation 3. At the end of charge, the Cu signal disappears and spinel $CuCo_2S_4$ re-forms while MgS and Co_9S_8 remain, suggesting that a combination of reversible and irreversible transitions are occurring, as is the case for WS-CuS. This naturally limits the charge capacity to 250 mAh g^{-1}, although subsequent discharge recovered almost all of that capacity (**Figure S4**). However, continuous cycling resulted in capacity fade. In-depth electrochemical characterization of individual processes will be the subject of future studies in order to identify the transitions mentioned above and assess their reversibility. While conversion cathodes traditionally suffer from rapid capacity fade, the direct preparation of nano-composite electrodes has been previously demonstrated as a viable technique to significantly improve the performance of many materials.[63–66] Indeed, we show here that this is the case for $CuCo_2S_4$, a novel Mg cathode material.

Conclusions:

Analysis of known Mg cathodes (TiS_2, CuS and Ti_2S_4) indicates that nano-sizing electrode materials provides several advantages due to shorter Mg^{2+} pathways and increased electrode-electrolyte contact. However, the method used to prepare nano-sized electrode materials also plays a crucial role governing overall electrochemical performance. Both intercalation materials, WS-TiS_2 and BM-Ti_2S_4, achieve more stable capacity retention when nano-sized since the smaller grains reduce cation trapping within the lattice and buffer the volume change during cycling. However, despite its enhanced reversibility, BM-Ti_2S_4 delivers a lower initial capacity in comparison to bulk material. Nano-sizing also benefits conversion materials, as interaction with the electrolyte is promoted and additional nucleation sites are created for phase transformation, allowing cathodes to function at lower temperatures. Optimal results are achieved when nanomaterials are synthesized directly, rather than reducing particle size of bulk material since high-energy methods such as ball milling can damage the structure of the active material and negatively impact electrochemical performance.

Despite issues with nano-sized electrodes, such as decreasing volumetric capacities and enhancing side reactions,[67,38] the current stage of Mg cathode research requires the identification of more potential compounds and the improvement of the electrochemical performance of existing cathodes. This work demonstrates that nano-sizing electrode materials prior to electrochemical characterization may be crucial so that successful candidates are not overlooked. When micron-sized $CuCo_2S_4$ was prepared using conventional methods, it appears electrochemically inert at most temperatures and only delivers a low (60 mAh g^{-1}) capacity at 150 °C. Ball milling to reduce particle size provides a rapid and useful technique to gain insight into the material's true potential; however,

negative side-effects of this method limit the capacity attained by the nanomaterial. BM-$CuCo_2S_4$ shows significantly more promising results in comparison to bulk material (delivering 180 mAh g^{-1} at only 60 °C), but nano-sized X-$CuCo_2S_4$ prepared directly from a low temperature xanthate salt melt exhibits the best performance by far (350 and 140 mAh g^{-1} at 60 °C and room temperature, respectively). Thus, developing synthetic techniques to directly crystallize nano-sized sulfide materials may be critical in the discovery and design of novel Mg electrodes.

Experimental Methods:

Nano-sized TiS_2 was obtained *via* the wet synthesis proposed by Jeong, *et al*.[54] In a 100 mL round bottom flask, $TiCl_4$ (880 µL) was added to oleylamine (12 g) and heated to 300 °C under magnetic stirring and N_2 flow. Then CS_2 (1.56 mL) was injected into the mixture, which immediately turned black upon addition. The temperature was held at 300 °C for 15 minutes to allow for the completion of the reaction. The flask was transferred to an Ar-filled glovebox after naturally cooling to room temperature, and the product was collected by filtration and washed with butanol and a mixture of 3:1 volume ratio methanol:hexane.

Nano-sized CuS was synthesized by the method reported by Pradhan, *et al*.[55] Typically, $Cu(NO_3)_2 \cdot 3H_2O$ (2.42 g) was dissolved in ethylene glycol (EG) (200 mL), and $Na_2S_2O_3$ (1.58 g) was then added. The mixture was stirred at room temperature for 20 minutes followed by 70 °C for four hours. After cooling to room temperature, the product was collected by filtration and washed with water and ethanol.

The synthesis of micron-sized spinel Ti_2S_4 was described in our previous publication,[30] and mechanical ball milling was then carried out to reduce the particle size. In an Ar-filled glovebox, Ti_2S_4 (1 g) power and acetonitrile (ACN, 1.5 mL) were added to a 15 mL ZrO_2 jar containing 5 mm ZrO_2 balls (12 g), followed by a milling period of 4 hours at 30 Hz with a Pulverisette 23 mini-miller. The solid was collected after evaporation of the ACN solvent.

Micron-sized $CuCo_2S_4$ was synthesized by mixing the elements in stoichiometric ratios which were then sealed in an evacuated quartz tube and heated at 450 °C for three days. The particle size was reduced by ball milling material (200 mg) in a 15 mL ZrO_2 jar containing 5 mm ZrO_2 balls (8 g) and NMP (750 mg) at 30 Hz for two hours. Nano-sized $CuCo_2S_4$ was synthesized directly through a low temperature melt of ethylxanthate salts reported by Khan *et al*.[62] A stoichiometric mixture of copper(I) ethylxanthate and cobalt(II) ethylxanthate was heated to 250 °C under Ar flow for one hour. The X-$CuCo_2S_4$ product was transferred to an Ar-filled glovebox after naturally cooling to room temperature.

X-ray diffraction (XRD) analysis was carried out on a PANalytical Empyrean diffractometer with Cu-Kα or Co-Kα radiation. Material morphologies were examined using a Zeiss field emission scanning electron microscope (SEM) equipped with an energy dispersive X-ray spectroscopy detector (EDX). X-ray photoelectron spectroscopy (XPS) was carried out on a Thermo VG Scientific ESCLab 250 instrument.

The spinel Ti_2S_4, layered TiS_2 and $CuCo_2S_4$ cathodes were prepared in an Ar-filled glovebox by mixing the as-prepared materials with Super P and polyvinyldiene fluoride (PVDF, average Mw ~534,000) in an 8:1:1 weight ratio in N-methyl-2-pyrrolidone (NMP) and casting the slurry onto Mo foil, while a weight ratio of 6:3:1 mixed in air and a carbon paper current collector was used for the CuS material. The APC electrolyte was synthesized following the reported procedure, with tetrahydrofuran (THF) or tetraglyme (G4) as the solvent.[32,68] Magnesium metal was polished with carbide paper (Mastercraft®, 180 grit SiC) and cleaned with a Kimwipe prior to use. Coin cells (2325) with Mg counter electrodes were used for cycling studies. All cell assembly and most electrode preparation was carried out in an Ar-filled glovebox, with the exception of CuS electrodes which were prepared in air. All electrochemistry was performed with a VMP3 potentiostat/galvanostat (Bio-logic).

In-situ XRD measurements for CuS were carried out by casting the cathode slurry on a glassy carbon electrode, which was then assembled in a home-made *in situ* cell with APC electrolyte and Mg metal anode. The cell was cycled at 30 mA g^{-1} and room temperature, with XRD scans recorded *operando*. Each scan was 30 min, corresponding to 15 mAh g^{-1} capacity or $\Delta x = 0.0268$ in Mg_xCuS.

Associated Content:

Supporting Information

The Supporting Information is available free of charge on *** website at DOI:

Additional information: ***

Author Information:

Corresponding Author

*lfnazar@uwaterloo.ca

Notes

The authors declare no competing financial interest

Acknowledgments:

This work was supported by the Joint Center for Energy Storage Research (JCESR), an Energy Innovation Hub funded by the US Department of Energy (DOE), Office of Science, Basic Energy Sciences. NSERC is acknowledged by L.F.N. for a Canada Research Chair and for funding through the NSERC Discovery Grants program.

References:

[1] Z. Yang, J. Zhang, M. C. W. Kintner-Meyer, X. Lu, D. Choi, J. P. Lemmon, J. Liu, *Chem. Rev.* **2011**, *111*, 3577.

[2] M. R. Palacín, *Chem. Soc. Rev.* **2009**, *38*, 2565.

[3] J. Liu, J.-G. Zhang, Z. Yang, J. P. Lemmon, C. Imhoff, G. L. Graff, L. Li, J. Hu, C. Wang, J. Xiao, G. Xia, V. V. Viswanathan, S. Baskaran, V. Sprenkle, X. Li, Y. Shao, B. Schwenzer, *Adv. Funct. Mater.* **2013**, *23*, 929.

[4] J. Cabana, L. Monconduit, D. Larcher, M. R. Palacín, *Adv. Mater.* **2010**, *22*, E170.

[5] L. Wen, J. Liang, J. Chen, Z.-Y. Chu, H.-M. Cheng, F. Li, *Small Methods* **2019**, *3*, 1900323.

[6] A. El Kharbachi, O. Zavorotynska, M. Latroche, F. Cuevas, V. Yartys, M. Fichtner, *J. Alloys Compd.* **2020**, *817*, 153261.

[7] M. Fichtner, *Magnesium Batteries: Research and Applications*; Royal Society of Chemistry, **2019**.

[8] A. Ponrouch, M. R. Palacín, *Philos. Transact. A Math. Phys. Eng. Sci.* **2019**, *377*, 20180297.

[9] H. D. Yoo, I. Shterenberg, Y. Gofer, G. Gershinsky, N. Pour, D. Aurbach, *Energy Environ. Sci.* **2013**, *6*, 2265.

[10] J. Muldoon, C. B. Bucur, T. Gregory, *Chem. Rev.* **2014**, *114*, 11683.

[11] P. Canepa, G. Sai Gautam, D. C. Hannah, R. Malik, M. Liu, K. G. Gallagher, K. A. Persson, G. Ceder, *Chem. Rev.* **2017**, *117*, 4287.

[12] J. Muldoon, C. B. Bucur, T. Gregory, *Angew. Chem. Int. Ed Engl.* **2017**, *56*, 12064.

[13] A. L. Lipson, S.-D. Han, B. Pan, K. A. See, A. A. Gewirth, C. Liao, J. T. Vaughey, B. J. Ingram, *J. Electrochem. Soc.* **2016**, *163*, A2253.

[14] K. Ta, K. A. See, A. A. Gewirth, *J. Phys. Chem. C* **2018**, *122*, 13790.

[15] Z. Zhao-Karger, M. E. G. Bardaji, O. Fuhr, M. Fichtner, *J. Mater. Chem. A* **2017**, *5*, 10815.

[16] K. A. See, K. W. Chapman, L. Zhu, K. M. Wiaderek, O. J. Borkiewicz, C. J. Barile, P. J. Chupas, A. A. Gewirth, *J. Am. Chem. Soc.* **2016**, *138*, 328.

[17] S. S. Kim, S. C. Bevilacqua, K. A. See, *ACS Appl. Mater. Interfaces* **2019**.

[18] M. S. Whittingham, C. Siu, J. Ding, *Acc. Chem. Res.* **2018**, *51*, 258.

[19] E. Levi, M. D. Levi, O. Chasid, D. Aurbach, *J. Electroceramics* **2009**, *22*, 13.

[20] E. Levi, Y. Gofer, D. Aurbach, *Chem. Mater.* **2010**, *22*, 860.

[21] L. F. Wan, B. R. Perdue, C. A. Apblett, D. Prendergast, *Chem. Mater.* **2015**, *27*, 5932.

[22] D. Kundu, S. H. Vajargah, L. Wan, B. Adams, D. Prendergast, L. F. Nazar, *Energy Environ. Sci.* **2018**, *11*, 881.

[23] D. S. Tchitchekova, D. Monti, P. Johansson, F. Bardé, A. Randon-Vitanova, M. R. Palacín, A. Ponrouch, *J. Electrochem. Soc.* **2017**, *164*, A1384.

[24] T. S. Arthur, R. Zhang, C. Ling, P.-A. Glans, X. Fan, J. Guo, F. Mizuno, *ACS Appl. Mater. Interfaces* **2014**, *6*, 7004.

[25] C. Ling, R. Zhang, T. S. Arthur, F. Mizuno, *Chem. Mater.* **2015**, *27*, 5799.

[26] X. Sun, V. Duffort, B. L. Mehdi, N. D. Browning, L. F. Nazar, *Chem. Mater.* **2016**, *28*, 534.

[27] C. Ling, R. Zhang, F. Mizuno, *ACS Appl. Mater. Interfaces* **2016**, *8*, 4508.

[28] R. Zhang, C. Ling, *ACS Appl. Mater. Interfaces* **2016**, *8*, 18018.

[29] D. Aurbach, Z. Lu, A. Schechter, Y. Gofer, H. Gizbar, R. Turgeman, Y. Cohen, M. Moshkovich, E. Levi, *Nature* **2000**, *407*, 724.

[30] X. Sun, P. Bonnick, V. Duffort, M. Liu, Z. Rong, K. A. Persson, G. Ceder, L. F. Nazar, *Energy Environ. Sci.* **2016**, *9*, 2273.

[31] X. Sun, P. Bonnick, L. F. Nazar, *ACS Energy Lett.* **2016**, *1*, 297.

[32] V. Duffort, X. Sun, L. F. Nazar, *Chem. Commun. Camb. Engl.* **2016**, *52*, 12458.

[33] C. Delacourt, P. Poizot, M. Morcrette, J.-M. Tarascon, C. Masquelier, *Chem. Mater.* **2004**, *16*, 93.

[34] C. Delacourt, L. Laffont, R. Bouchet, C. Wurm, J.-B. Leriche, M. Morcrette, J.-M. Tarascon, C. Masquelier, *J. Electrochem. Soc.* **2005**, *152*, A913.

[35] J. Liu, J. Wang, Y. Ni, Y. Zhang, J. Luo, F. Cheng, J. Chen, *Small Methods* **2019**, *3*, 1900350.

[36] D. Monti, A. Ponrouch, M. Estruga, M. R. Palacín, J. A. Ayllón, A. Roig, *J. Mater. Res.* **2013**, *28*, 340.

[37] P. Poizot, S. Laruelle, S. Grugeon, L. Dupont, J.-M. Tarascon, *Nature* **2000**, *407*, 496.

[38] M. S. Whittingham, *Dalton Trans.* **2008**, 5424.

[39] T. Jiang, R. Zhang, Q. Yin, W. Zhou, Z. Dong, N. A. Chernova, Q. Wang, F. Omenya, M. S. Whittingham, *J. Mater. Sci.* **2017**, *52*, 3670.
[40] J. Ni, Y. Zhao, L. Li, L. Mai, *Nano Energy* **2015**, *11*, 129.
[41] Y. Ren, Z. Liu, F. Pourpoint, A. R. Armstrong, C. P. Grey, P. G. Bruce, *Angew. Chem. Int. Ed.* **2012**, *51*, 2164.
[42] D. Herrera-Miranda, A. Ponrouch, J. Pons, C. Domingo, M. R. Palacín, J. A. Ayllón, *Mater. Res. Bull.* **2012**, *47*, 2369.
[43] E. Lancry, E. Levi, Y. Gofer, M. D. Levi, D. Aurbach, *J. Solid State Electrochem.* **2005**, *9*, 259.
[44] Y. Cheng, L. R. Parent, Y. Shao, C. Wang, V. L. Sprenkle, G. Li, J. Liu, *Chem. Mater.* **2014**, *26*, 4904.
[45] H. Tang, F. Xiong, Y. Jiang, C. Pei, S. Tan, W. Yang, M. Li, Q. An, L. Mai, *Nano Energy* **2019**, *58*, 347.
[46] L. Hu, I. D. Johnson, S. Kim, G. M. Nolis, J. W. Freeland, H. D. Yoo, T. T. Fister, L. McCafferty, T. E. Ashton, J. A. Darr, J. Cabana, *Nanoscale* **2019**, *11*, 639.
[47] C. Kim, A. A. Adil, R. D. Bayliss, T. L. Kinnibrugh, S. H. Lapidus, G. M. Nolis, J. W. Freeland, P. J. Phillips, T. Yi, H. D. Yoo, B. J. Kwon, Y.-S. Yu, R. Klie, P. J. Chupas, K. W. Chapman, J. Cabana, *Chem. Mater.* **2018**, *30*, 1496.
[48] P. Kulkarni, S. K. Nataraj, R. G. Balakrishna, D. H. Nagaraju, M. V. Reddy, *J. Mater. Chem. A* **2017**, *5*, 22040.
[49] M. M. Butala, M. A. Perez, S. Arnon, C. Göbel, M. B. Preefer, R. Seshadri, *Solid State Sci.* **2017**, *74*, 8.
[50] G. M. Nolis, J. M. Bolotnikov, J. Cabana, *Inorg. Chem.* **2018**.
[51] S. Grugeon, S. Laruelle, R. Herrera-Urbina, L. Dupont, P. Poizot, J.-M. Tarascon, *J. Electrochem. Soc.* **2001**, *148*, A285.
[52] A. Ponrouch, M. R. Palacín, *J. Power Sources* **2012**, *212*, 233.
[53] N.-W. Li, Y.-X. Yin, S. Xin, J.-Y. Li, Y.-G. Guo, *Small Methods* **2017**, *1*, 1700094.
[54] S. Jeong, D. Yoo, J. Jang, M. Kim, J. Cheon, *J. Am. Chem. Soc.* **2012**, *134*, 18233.
[55] J. Kundu, D. Pradhan, *ACS Appl. Mater. Interfaces* **2014**, *6*, 1823.
[56] Z. Zhang, S. Dong, Z. Cui, A. Du, G. Li, G. Cui, *Small Methods* **2018**, *2*, 1800020.
[57] Z. Wang, S. Rafai, C. Qiao, J. Jia, Y. Zhu, X. Ma, C. Cao, *ACS Appl. Mater. Interfaces* **2019**, *11*, 7046.
[58] Y. Zhang, Y. Li, Y. Wang, R. Guo, W. Liu, H. Pei, G. Yin, D. Ye, S. Yu, J. Xie, *J. Colloid Interface Sci.* **2019**, *553*, 239.
[59] M. Wu, Y. Zhang, T. Li, Z. Chen, S. Cao, F. Xu, *Nanoscale* **2018**, *10*, 12526.
[60] K. V. Kravchyk, R. Widmer, R. Erni, R. J.-C. Dubey, F. Krumeich, M. V. Kovalenko, M. I. Bodnarchuk, *Sci. Rep.* **2019**, *9*, 7988.
[61] J. Rouxel, M. Tournoux, *Solid State Ion.* **1996**, *84*, 141.
[62] M. Dilshad Khan, G. Murtaza, N. Revaprasadu, P. O'Brien, *Dalton Trans.* **2018**, *47*, 8870.
[63] P. Nie, G. Xu, J. Jiang, H. Dou, Y. Wu, Y. Zhang, J. Wang, M. Shi, R. Fu, X. Zhang, *Small Methods* **2018**, *2*, 1700272.
[64] B. P. Vinayan, Z. Zhao-Karger, T. Diemant, V. S. Kiran Chakravadhanula, N. I. Schwarzburger, M. Ali Cambaz, R. Jürgen Behm, C. Kübel, M. Fichtner, *Nanoscale* **2016**, *8*, 3296.
[65] D. Wang, R. Kou, D. Choi, Z. Yang, Z. Nie, J. Li, L. V. Saraf, D. Hu, J. Zhang, G. L. Graff, J. Liu, M. A. Pope, I. A. Aksay, *ACS Nano* **2010**, *4*, 1587.
[66] Z. Li, S. Liu, B. P. Vinayan, Z. Zhao-Karger, T. Diemant, K. Wang, R. J. Behm, C. Kübel, R. Klingeler, M. Fichtner, *Energy Storage Mater.* **2019**, *21*, 115.
[67] Y. Wang, H. Li, P. He, E. Hosono, H. Zhou, *Nanoscale* **2010**, *2*, 1294.
[68] O. Mizrahi, N. Amir, E. Pollak, O. Chusid, V. Marks, H. Gottlieb, L. Larush, E. Zinigrad, D. Aurbach, *J. Electrochem. Soc.* **2008**, *155*, A103.

Table of Contents:

ToC Text:

The method of preparation of nano-sized electrode materials plays a key role in their observed electrochemistry, where optimal performance is obtained through direct nano-synthesis techniques rather than mechanical milling methods. Developing such nano-synthetic routes can lead to the discovery of novel Mg cathode materials - such as $CuCo_2S_4$ - that might otherwise be overlooked when screening for new candidates.

ToC Figure:

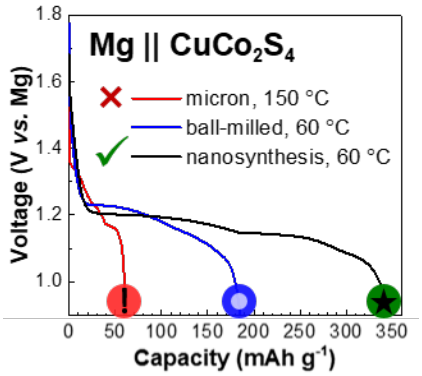

ToC keyword: nano-synthesis